

The influence of added nano carbon black on the electrical properties of the cathode of a lithium-ion secondary battery

Ying-Ni Luo^a, Yuo-Tern Tsai^b and Kuan-Hong Lin^{a,*}

^aDepartment of Mechanical Engineering, Tunghan University, New Taipei City 222, Taiwan, ROC

^bDepartment of Mechanical Engineering, De-Lin Institute of Technology, New Taipei City 236, Taiwan, ROC

The cathode of a lithium-ion secondary battery was fabricated using lithium iron phosphate blended with nano carbon black. The effects of four kinds of carbon black on lithium iron phosphate were evaluated by irreversible capacity loss and cycling performance. Analyses results show that the specimen 1B had the lowest irreversible capacity loss at charge-discharge cycling rate 1C among all of the specimens to which 1 wt.% carbon black was added. All of the specimens had a lower charge-discharge capacity at cycling rate 1C and a higher charge-discharge capacity at cycling rate C/2. Cycling performance test results indicated that the specimen 1B had the highest discharge-capacity and the lowest fade rate.

Key words: Lithium iron phosphate, Carbon black, Capacity, Cycling performance.

Introduction

The cathode materials of lithium-ion secondary batteries consist of transition metal oxides, such as LiFePO₄, LiCoO₂, LiNiO₂, Li(Ni_{0.8}Co_{0.2})O₂, and spinel LiMn₂O₄, among others [1-5]. Phospho-olivine lithium iron phosphate (LiFePO₄) is a promising cathode material for lithium rechargeable batteries. The advantages of LiFePO₄ include the following: a large theoretical capacity of 170 mAh/g, rapid chargeability, good cycle stability, thermal stability in a fully charged state, environmental benignity, and inexpensiveness. In addition, LiFePO₄ is light weight and has a high power density and good recycle life compared with the other cathode materials [6-8]. However, it is difficult to attain its full capacity because its electronic conductivity is very low at room temperature; it also exhibits slow kinetics of lithium-ion diffusion through the LiFePO₄-FePO₄ interfaces. For this reason, methods to improve LiFePO₄ materials to a superior state require charging at low current densities or high temperatures [9].

Several approaches have been adopted to improve the electronic conductivity of LiFePO₄ materials. These approaches include coating high electronic conductive elements such as carbon, silver, and copper onto the LiFePO₄ [1, 7, 9], adding carbon black substance [6, 10-12] or doping with high valence metal ions [1-3, 7], and minimizing the particle size of the LiFePO₄ [13-14]. The small particle size and large specific surface area of carbon black make it the preferred

choice in electric conduction. The addition of carbon black into lithium iron phosphate promotes the electron transfer speed and also increases the charge-discharge performance of the cell. The electronic conductivity of carbon black is higher than that of cathode materials; accordingly, it results in decreases in electric resistance and heat, while also promoting the cycle life and safety of the cell. However, due to the effect of Van der Waals forces, the low densities in carbon black dispersion are difficult in a cathode material, which in turn may cause irregular electric resistance and decreased cell performance [6, 10].

In this study, we assembled the cathode materials with LiFePO₄ and different kinds of carbon black. The effects of carbon black on the capacity and cycling performance of the lithium-ion cell are reported, and the optimal addition amount and variety of carbon black are suggested according to the experimental results.

Experimental Procedure

LiFePO₄ (Tron energy technology, IPC 11201011) was used as the cathode material in lithium-ion secondary batteries. Four different characteristic nano carbon blacks designated as A (Taiwan maxwave, Super P Li), B (China synthetic rubber co., C003), D (China synthetic rubber co., C007), and E (Taiwan maxwave, ENSACO 350G), respectively, were added into LiFePO₄ materials. The designation number and composition of the cathode specimens are listed in Table 1.

LiFePO₄ was first blended with nano carbon black according to the composition show in Table 1. An N-Methyl-2-pyrrolidone (NMP, Taiwan maxwave) was used as solvent and 5 wt.% polyvinylidene fluoride

*Corresponding author:
Tel : +886-2-8662-5917
Fax: +886-2-8662-5919
E-mail: khlin@mail.tnu.edu.tw

Table 1. Designation and composition of cathode specimens.

Cathode specimen	LiFePO ₄ (wt.%)	Nano carbon black (wt.%)				PVDF (wt.%)
		A	B	D	E	
M	95.0					5.0
1A	94.0	1.0				5.0
1B	94.0		1.0			5.0
1D	94.0			1.0		5.0
1E	94.0				1.0	5.0
3A	92.0	3.0				5.0
5A	90.0	5.0				5.0
0.5B	94.5		0.5			5.0
0.5E	94.5				0.5	5.0

(PVDF) as binder. After a stirred process the slurry was spread on the aluminum foil and then dried in an oven for 60 min at 150 °C. Subsequently, it was pressed with a pressure of 5 MPa, and finally cut into a circular sheet with 10 mm diameter as the cathode specimen. The coin-cell structure and the method employed to fabricate the electrode sheet and the cell were similar to those used for commercially available cells. The electrolyte consisted of ethylene carbonate/diethyl carbonate and LiPF₆, and a separator was adopted to prevent the short circuits caused by the anode and cathode touching.

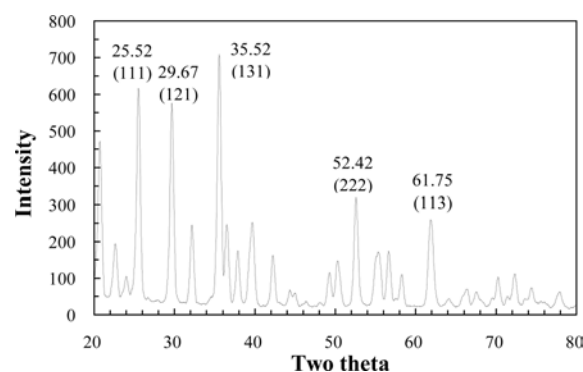
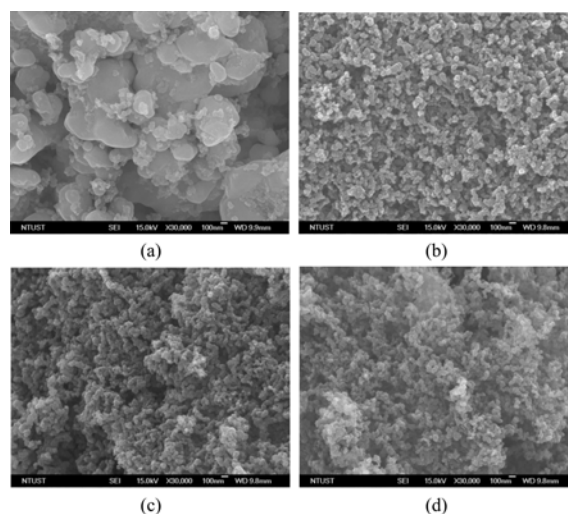
The crystal structure of the carbon black and LiFePO₄ were analyzed using an X-ray diffractometer (Shimadzu, XRD-6000) at 30 kV and 30 mA with CuK α ($\lambda = 0.15418$ nm) radiation. The scanning range (2θ) was set from 20° to 80° with a scan rate of 2°/min. A field emission scanning electron microscope (FE-SEM, Jeol, JSM-6500F) with an operating voltage of 15 kV was used to inspect the carbon black, LiFePO₄, and cathode specimen. A Brenauer-Emmett-Teller adsorption analyzer (BET, Micromeritics, AccuPyc II 1340) was used to determine the specific surface area of carbon black. A four-point probe sheet resistance meter (TM technology, FPSR100) was used to measure the conductivity of the cathode specimen.

A constant current charge-discharge profile of the coin-cell was recorded by a battery test system (Maccor, 4000) with a cycling rate C/2, and 1C, cut off voltage 4.2 V, and 2 V, respectively. Cycling performance was performed for 34 times in total. The 1st to 2nd cycle adopted C/10 rate, and the 3rd to 4th cycle adopted C/2 rate for battery formation. The 5th to 34th cycle adopted 1C rate; recording the variation of current and voltage with time. The charge and discharge capacities (mAh/g) in each cycle were calculated. The discharge cycle proceeded after 10 min of the charge cycle and the cut off voltage was 2V.

Results and Discussion

Cathode specimens

Fig. 1 shows the XRD pattern of LiFePO₄ powders.

**Fig. 1.** XRD pattern of the LiFePO₄ powders.**Fig. 2.** SEM images of powders: (a) LiFePO₄, (b) carbon black A, (c) carbon black B, and (d) carbon black E.

The Miller indices corresponding to each peak in the diffraction pattern demonstrate a specific set of planes in the LiFePO₄ phase (JCPDS 40-1499). The lattice constants were calculated by solving four equations derived from the diffracted angles of (111), (121), (031), and (131) planes, assuming an orthorhombic structure. A least square regression of the four equations yielded the lattice constants of $a = 0.600$ nm, $b = 1.034$ nm, and $c = 0.469$ nm, which were similar to those found by E.M. Jin et al. [15]. In addition, XRD analysis shows that all of the carbon black powders with an orthorhombic crystal structure (JCPDS 89-8491) and similar lattice constants were as follows: $a = 0.407$ nm, $b = 0.505$ nm, and $c = 0.645$ nm.

Fig. 2 show the scanning electron microscope (SEM) images of LiFePO₄ and carbon black powders. Fig. 2(a) shows that the larger powders were LiFePO₄, and the particles smaller than 100 nm were carbon black. Figs. 2(b-d) illustrate the secondary electron images (SEI) of carbon black A, B, and E, respectively. These figures revealed not only the spheroid shape but also a serious agglomerate phenomenon of carbon black. Such a phenomenon could be ascribed to the low density of the carbon black; thus, dispersion is difficult

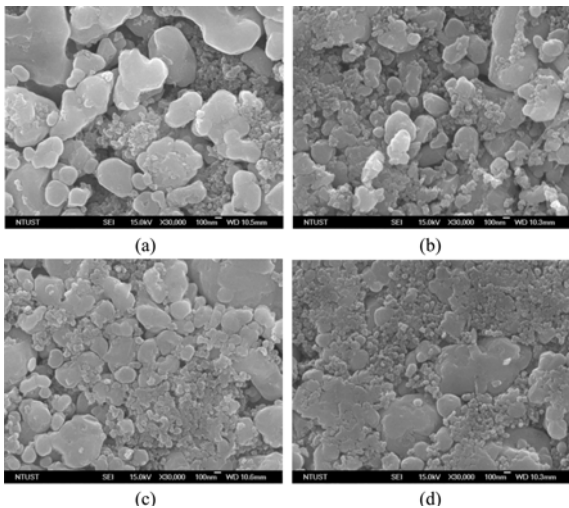


Fig. 3. SEM images of the cathode specimens: (a) 1A, (b) 3A, (c) 5A, and (d) 1E.

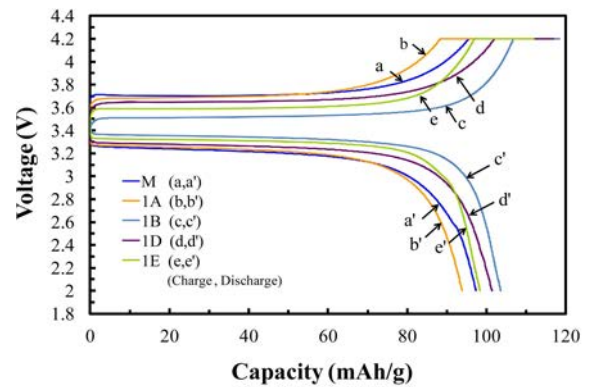
due to the effect of Van der Waals forces.

The Brenauer-Emmett-Teller (N_2 -BET) adsorption method was used for measuring the specific surface area of the carbon black powders. The specific surface area of the carbon black A, B, D, and E were $61.5 \text{ m}^2/\text{g}$, $786.0 \text{ m}^2/\text{g}$, $90.9 \text{ m}^2/\text{g}$, and $798.1 \text{ m}^2/\text{g}$, respectively. It is particularly noteworthy that the specific surface area difference between these carbon black powders was 13 times maximally, probably because the various vendors of the carbon black employed a different manufacturing process. Some of the processes approve carbon black with micro-voids and thus increase the specific surface area substantially. It can be observed in Figs. 2(c) and 2(d) that carbon black B and E demonstrates a loosened appearance.

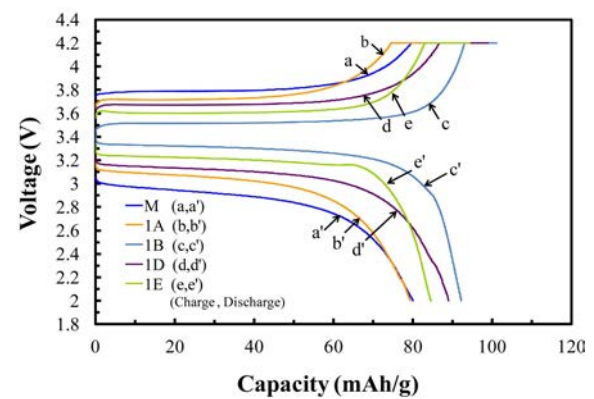
Figs. 3(a-d) show the secondary electron images of the cathode specimens 1A, 3A, 5A, and 1E, which were added with 1 wt.%, 3 wt.%, 5 wt.% of A carbon black, and 1 wt.% of E carbon black into the LiFePO_4 , respectively. It was found that after an increase in A carbon black, the agglomerate phenomenon become very pronounced. Such a trend was believed to arise from the effect of Van der Waals force, as previously mentioned. This was probably due to the fact that the fabrication process of the cathode specimen followed a commercial process that includes insufficient mixes and a slowly agitated speed. In addition, even though the addition amount was only 1 wt.%, the agglomerate phenomenon of carbon black in the 1E specimen was very pronounced. This can be attributed to the high specific surface area of the E carbon black. The inadequate dispersion of carbon black may be harmful to the electric capacity of the cathode specimen.

Performance test of cell

Five coin-cells that used M, 1A, 1B, 1D, and 1E cathode specimens processed a charge-discharge test at cycling rate $C/2$ and $1C$, respectively. The charge cycle



(a)



(b)

Fig. 4. Charge-discharge profiles at the first cycle of specimens M, 1A, 1B, 1D, and 1E, the cycling rate: (a) $C/2$, (b) $1C$, cut off voltage 4.2 V, and 2 V.

Table 2. Irreversible capacity loss of various specimens at $C/2$ and $1C$ cycling rate.

Cathode specimen	Conductivity (S/m)	Charge/Discharge (mAh/g) ($C/2$)	Irr. % ($C/2$)	Charge/Discharge (mAh/g) ($1C$)	Irr. % ($1C$)
M	0.56	111.2/97.3	12.5	94.1/81.8	13.1
1A	1.06	106.4/93.8	11.8	89.0/79.3	10.9
1B	5.47	118.3/103.5	12.5	101.2/92.2	8.9
1D	1.07	116.8/101.4	13.2	99.0/89.1	10.0
1E	5.15	111.9/98.4	12.1	94.4/85.5	9.4
3A	3.14	106.7/95.9	10.1	93.3/85.7	8.2
5A	3.16	111.1/99.7	10.3	97.7/89.9	8.0
0.5B	1.13	109.9/96.1	12.6	94.1/85.0	9.7
0.5E	1.19	105.4/91.1	13.6	89.1/80.1	10.0

adopted a constant-current mode at first, until the voltage reached 4.2 V, at which time it changed to a constant-voltage mode. This voltage was applied to the cell until the electric current was decreased to tenth of its initial value. The discharge cycle was initiated after 10 min of the charge cycle; a constant-current mode was adopted, and the cut off voltage was 2 V. The

variations of current and voltage with time were recorded, and the charge and discharge capacities (mAh/g) were calculated.

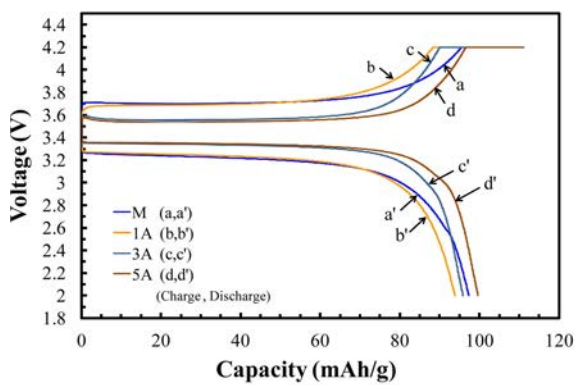
Figs. 4(a) and 4(b) show the charge and discharge profiles at the first cycle of five coin-cells with cycling rate C/2 and 1C, respectively. All of the profiles show a flat voltage curve with a plateau around 3.4 V, which indicate the excellent stability of the cells. The difference between the charge and discharge capacity at the first cycle was defined as irreversible capacity loss (Irr. %), as illustrated in Table 2.

Table 2 shows that the conductivity of specimens 1B (5.47 S/m) and 1E (5.15 S/m) were approximately ten times higher than M (0.56 S/m) and approximately five times than the 1A (1.06 S/m) and 1D (1.07 S/m). These results were possibly caused because a large specific surface area carbon black B and E were added to the 1B and 1E specimens and thus had a higher level of conductivity. In addition, the conductivity of specimen 3A (3.14 S/m) was around three times higher than 1A (1.06 S/m); however, the conductivity of specimen 5A (3.16 S/m) was not higher than 1A five times proportionally. This trend was believed to arise either

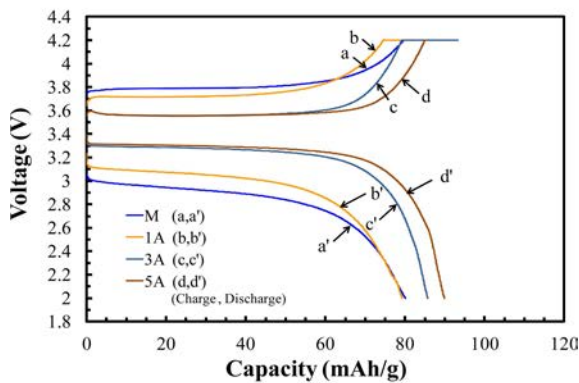
from the inadequate dispersion of carbon black in the cathode specimen or because the additional amount of carbon black resulted in over-saturation.

The irreversible capacity loss of specimen 1A was only lower than that of specimen M 0.7% at C/2 cycling rate. However, the irreversible capacity loss of the specimen 1A was lower than that of specimen M 2.2%; and, 1B was lower than that of specimen M 4.2% at 1C cycling rate, respectively. The excellent performance of specimen 1B was caused by the porosity of the carbon black that provides a storage space for the electrolyte and thus promotes the shift of Li-ion between the electrodes at a high cycling rate [16]. It was also observed that the cycling rate increased and the utilization of the active material decreased, thus resulting in decreases in charge and discharge capacity; this finding corresponded with the findings of previous studies [16-17].

Figs. 5(a) and 5(b) show the charge and discharge profiles at the first cycle of four coin-cells with cycling rate C/2 and 1C, respectively. At cycling rate C/2, the difference of irreversible capacity loss between the specimens M and 1A, 3A, 5A was 0.7%, 2.4%, and

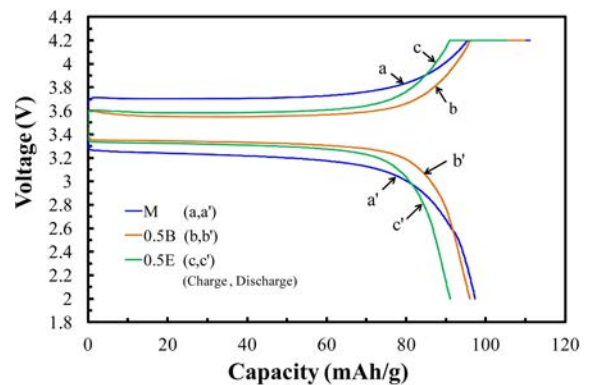


(a)

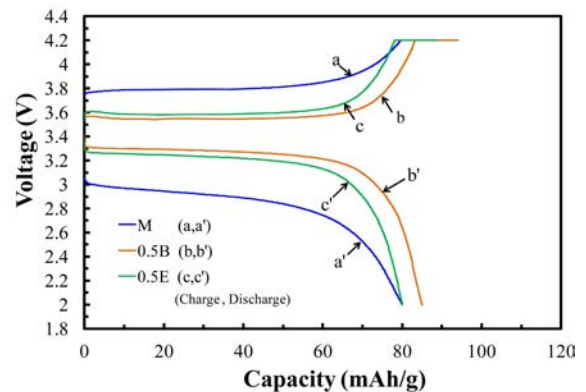


(b)

Fig. 5. Charge-discharge profiles at the first cycle of specimens M, 1A, 3A, and 5A, the cycling rate: (a) C/2, (b) 1C, cut off voltage 4.2 V, and 2 V.

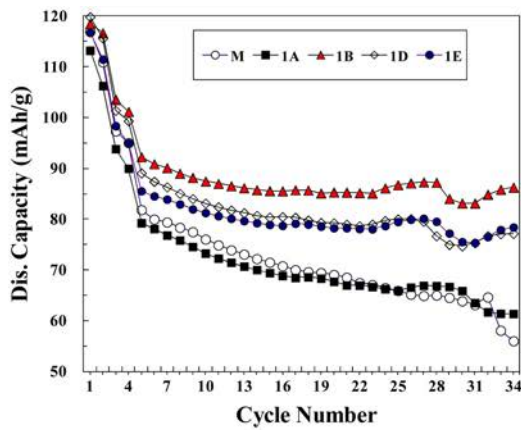


(a)

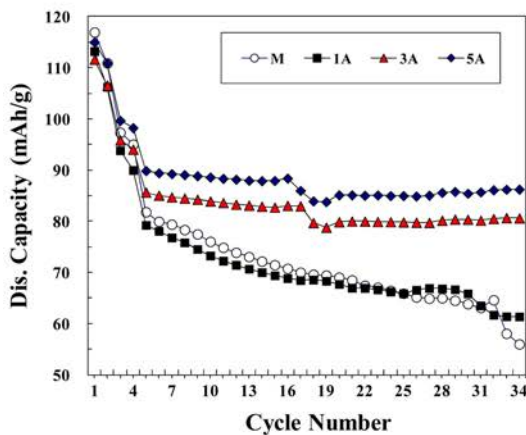


(b)

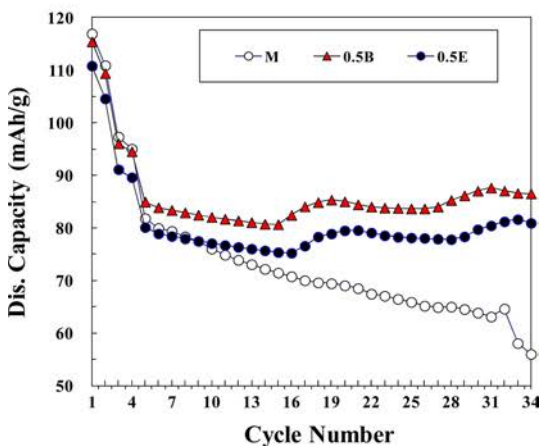
Fig. 6. Charge-discharge profiles at the first cycle of specimens M, 0.5B, and 0.5E, the cycling rate: (a) C/2, (b) 1C, cut off voltage 4.2 V, and 2 V.



(a)



(b)



(c)

Fig. 7. Discharge capacity retention of the specimens: (a) M, 1A, 1B, 1D, 1E, (b) M, 1A, 3A, 5A, and (c) M, 0.5B, 0.5E versus cycle number.

2.2%, respectively. It is obvious that the addition of 3% to 5% A carbon black contributed to reduce the irreversible capacity loss even at a low cycling rate. At

cycling rate 1C, the difference of irreversible capacity loss between the specimens M and 1A, 3A, 5A was 2.2%, 4.9%, and 5.1%, respectively. This observation indicates that a higher cycling rate 1C and a higher amount of added A carbon black contribute to decreasing the irreversible capacity loss efficiently.

Figs. 6(a) and 6(b) show the charge and discharge profiles at the first cycle of specimens M, 0.5B, and 0.5E with cycling rate C/2 and 1C, respectively. The difference of irreversible capacity loss between the specimens M and 0.5B was only 0.1% at cycling rate C/2. It is clear that the addition of 0.5% B carbon black into LiFePO_4 cannot reduce irreversible capacity loss efficiently at a low cycling rate. However, the difference of irreversible capacity loss between the specimens M and 0.5B, and 0.5E were 3.4% and 3.1% at cycling rate 1C, respectively. The results showed that the addition of 0.5 wt.% B and E carbon black greatly contributed to reducing the irreversible capacity loss at a higher cycling rate. This may be associated with the loose structure and surface porosity of the B and E carbon black; thus, the electron had a smooth route and good conductivity at a high cycling rate [18].

Cycling performance was performed 34 times in total. The 1st to 2nd cycle was conducted with a C/10 cycling rate and the 3rd to 4th cycle was conducted with a C/2 cycling rate for battery formation. The 5th to 34th cycle was conducted with a 1C cycling rate, cut off voltage was 4.2 V and 2 V, respectively, and the charge and discharge capacities (mAh/g) were calculated.

Fig. 7(a) shows the discharge capacity retention of specimens M, 1A, 1B, 1D, and 1E at various cycle numbers. The decrease percentage of discharge-capacity between the 5th and 34th cycle was defined as fade rate % in this study. Table 3 shows specimen M which, without the addition of carbon black, had the highest fade rate (31.5%); the specimen 1B had the lowest fade rate (6.4%) of all of five specimens. Due to the fact that specimen 1B was added with large specific surface area B carbon black, it had higher electric conductivity, lower discharge-capacity fade rate, and better cycling

Table 3. Conductivity and discharge capacity fade rate of specimens.

Cathode specimen	Conductivity (S/m)	5 th Dis. cap. (mAh/g)	34 th Dis. cap. (mAh/g)	Fade rate (%)
M	0.56	81.8	56.0	31.5
1A	1.06	79.3	61.4	22.6
1B	5.47	92.2	86.3	6.4
1D	1.07	89.1	77.1	13.5
1E	5.15	85.5	78.4	8.3
3A	3.14	85.7	80.6	6.0
5A	3.16	89.9	86.2	4.1
0.5B	1.13	85.0	86.5	-1.8
0.5E	1.19	80.1	80.9	-1.0

performance. In addition, the discharge-capacity of specimen 1B at the 5th and 34th cycle were 92.2 mAh/g and 86.3 mAh/g, respectively, which was the highest value among the five specimens. For this reason, LiFePO₄ added with 1 wt.% B carbon black had the best cycling performance in this study.

Fig. 7(b) shows the discharge capacity retention of specimens M, 1A, 3A, and 5A at various cycle numbers. Table 3 shows that the discharge-capacity fade rate of four specimens were 31.5%, 22.6%, 6.0%, and 4.1%, respectively. It could be observed that, with an increase of A carbon black, the discharge-capacity fade rate decreased accordingly and exhibited a better cycling performance. However, the difference of discharge-capacity fade rate between 3A and 5A specimens was not apparent, possibly due to the fact that the additional amount of 5 wt.% A carbon black resulted in over-saturation. A comparison of the discharge-capacity fade rate of specimens 1B and 5A demonstrates that the rate was higher in 1B (6.4%) than in 5A (4.1%) by 2.3%; however, both specimens had almost the same discharge capacity retention (86.3 mAh/g) at the 34th cycle. Consequently, the addition of 1 wt.% B carbon black into LiFePO₄ had almost the same effect as 5 wt.% A carbon black in the cycling performance test.

Fig. 7(c) shows the discharge capacity retention of specimens M, 0.5B, and 0.5E at various cycle numbers. After 34 times cycling the specimen 0.5B had the highest discharge capacity retention (86.5 mAh/g) among the three specimens, higher than that of the 0.5E specimen 5.6 mAh/g and the M specimen 30.5 mAh/g, respectively. It is noteworthy that the discharge capacity retention of specimens 0.5B and 0.5E at the 34th cycle was higher than at the 5th cycle. This can be attributed to the instability of the discharge-capacity during the initial cycle, which was also observed in previous studies [18-20]. In addition, the influence to the discharge-capacity of 0.5 wt.% B carbon black was almost the same as 5 wt.% A carbon black. Based on the above observations, it can be concluded that the effect of four kinds of nano carbon black in improving discharge-capacity was B > E > D > A.

Conclusions

All of the specimens show a flat voltage curve with a plateau around 3.4 V, which indicates the excellent stability of the cells in this study. With the same addition amount of 1 wt.%, specimen 1B had the lowest irreversible capacity loss at 1C cycling rate. The irreversible capacity loss decreased with an increase of

A carbon black; however, an addition amount higher than 3 wt.% resulted in over-saturation. The LiFePO₄ cathode materials added with 1 wt.% B carbon black had the highest conductivity and charge-discharge capacity, and the lowest irreversible capacity loss. The effect of four kinds of carbon black in reducing irreversible capacity loss was B > E > D > A.

Acknowledgments

The authors would like to thank the Tron Energy Technology Co., Ltd. (Taiwan) for the specimens supplied and for financially supporting this study.

References

1. S.S. Zhang, K. Xu and T.R. Jow, *J. Power Sources*. 159[1] (2006) 702-707.
2. S.Y. Chung, J.T. Bloking and Y.M. Chiang, *Nat. Mater.* 1 (2002) 123-128.
3. C. Ouyang, S. Shi, Z. Wang, X. Huang, and L. Chen, *Phys. Rev. B* 69 (2004) 104303.
4. H.H. Chang, C.C. Chang, C.Y. Su, H.C. Wu, M.H. Yang and N.L. Wu, *J. Power Sources*. 185[1] (2008) 466-472.
5. D. Aurbach, B. Markovsky, G. Salitra and E. Markevich, *J. Power Sources* 165[2] (2007) 491-499.
6. Y. Lin, M.X. Gao, D. Zhu, Y.F. Liu and H.G. Pan, *J. Power Sources* 184[2] (2008) 444-448.
7. B. Jin and H.B. Gu, *Solid State Ionics* 178 (2008) 1907-1914.
8. J. Shim and K. A. Striebel, *J. Power Sources* 119-121 (2003) 955-958.
9. N. Iltchev, Y. Chen, S. Okada and J.I. Yamaki, *J. Power Sources* 119-121 (2003) 749-754.
10. C.R. Sides, F. Croce, V.Y. Young, C.R. Martin and B. Scrosati, *Electrochem. Solid-State Lett.* 8[9] (2005) A484-A487.
11. P.S. Herle, B. Ellis, N. Coombs and L.F. Nazar, *Nat. Mater.* 3 (2004) 147-152.
12. A.K. Padhi, K.S. Nanjundaswamy and J.B. Goodenough, *J. Electrochem. Soc.* 144 (1997) 1188-1194.
13. C. Delacourt, P. Poizot, S. Levasseur and C. Masquelier, *Electrochem. Solid-State Lett.* 9[7] (2006) A352-A355.
14. D. Choi and P.N. Kumta, *J. Power Sources* 163[2] (2007) 1064-1069.
15. E. M. Jin, B. Jin, D.K. Jun, K.H. Park, H.B. Gu and K.W. Kim, *J. Power Sources* 178[2] (2008) 801-806.
16. H.C. Wu, C.Y. Su, D.T. Shieh, M.H. Yang and N.L. Wu, *Electrochem. Solid-State Lett.* 9[12] (2006) A537-A541.
17. J. Ying, M. Lei, C. Jiang, C. Wan, X. He, J. Li, Li W. and J. Ren, *J. Power Sources* 158[1] (2006) 543-549.
18. P.P. Prosini, D. Zane and M. Pasquali, *Electrochim. Acta.* 46[23] (2001) 3517-3523.
19. M. Takahashi, H. Ohtsuka, K. Akuto and Y. Sakurai, *J. Electrochem. Soc.* 152[5] (2005) A899- A904.
20. H. Yamane, M. Saitoh, M. Sano, M. Fujita, M. Sakata, M. Takada, E. Nishibori and N. Tanaka, *J. Electrochem. Soc.* 149[12] (2002) A1514-A1520.